



Generalized correlation for onset flooding velocity in vertical channels

A. Biton^{a,b}, E. Rabinovich^a, E. Gilad^{b,*}

^a Nuclear Research Center Negev (NRCN), P.O.Box 9001, Beer Sheva 84190, Israel

^b The Unit of Nuclear Engineering, Ben-Gurion University of the Negev, P.O.Box 653, Beer Sheva 8410501, Israel

ARTICLE INFO

Keywords:

Onset of flooding velocity
Vertical channel
Characteristic length
Two-phase flow
Annulus

ABSTRACT

Flooding due to gas-liquid counter-current flow might significantly impact engineering applications such as boilers, heat exchangers, and nuclear reactors. Despite the extensive body of literature, there is still a notable disagreement on the appropriate definition of the characteristic length regarding the onset flooding velocity in rectangular and annular channels. The primary motivation for this study is to examine which geometric dimension is the most suitable to predict the onset of flooding velocity. This study measured the onset of flooding velocity in one circular and two different annular channels. The channel geometries are considered such that the hydraulic diameter trend is inverse to the average circumference. The study's findings show that the hydraulic diameter cannot be used as a characteristic length for annular and rectangular channels to describe the onset flooding velocity. Instead, the average circumference for the annular channel and channel width for rectangular channels exhibit superior performances. The flooding air velocity was increased by increasing the average circumference of the annular channel or channel width for the rectangular channel. New Wallis-type generalized relationships are derived based on the wide range of channel geometries and dimensions. The novel generalized empirical correlation could be defined regardless of the channel geometry.

1. Introduction

In a vertical channel, the flooding phenomenon can occur under certain conditions of liquid-gas counter-current flow. These conditions are related to incipient partial delivery of the liquid, and the first droplet drifted upward and discharged from the channel by the gas flow are defined as the onset of flooding. An additional increase in the gas flow rate will increase the liquid flow upward. If the gas velocity becomes high enough, the liquid will not penetrate the channel, and the counter-current flow will occur upward. The onset of flooding is generally undesirable and may pose a danger for various engineering applications such as boilers, heat exchangers, and nuclear reactors. For example, during the Loss of Cooling Accident (LOCA) in a nuclear reactor, the Emergency Core Cooling Systems (ECCS) should flow water inside the fuel rod channels to cool the fuel elements and avoid temperature escalation. However, flooding might occur if there is a significant upward steam flow against the downward water flow. As a result, the fuel cladding temperature might increase up to the melting point temperature due to the residual heat in the fuel and the limited heat transfer. Many studies used air as the gas phase instead of steam [1–17]. Air-water components constitute a good approximation for steam-water

systems if the water enters the channel is saturated and enough steam is produced during the flooding.

The gas-phase onset flooding velocity depends on the channel geometry and dimensions, liquid and gas properties, and liquid phase input velocity. The literature presents numerous studies which have experimentally examined the effect of a variety of parameters on the flooding phenomenon, such as channel geometry (circular, annular, or rectangular) [5,8], channel length [6,8,10], pipe's end geometry (channel's entrance and exit geometry) [10,11], channel gap [6–8], channel width [6,8], fluid properties [11,14], cross-flow [7] and channel inclination angle [11]. Based on all these factors, empirical data for predicting two-phase flow behavior is often limited to the specific experimental conditions under which the measurements were made.

Many studies have been published on the subject of onset flooding prediction. According to the existing literature, there is a significant disagreement on the most appropriate definition of the characteristic length regarding rectangular and annular channels. Some studies proposed a channel gap (the small cross-section dimension) as a characteristic length for rectangular geometry [8,13]. In contrast, others preferred using the channel width (the large cross-section dimension) [6,8]. For annular geometry, one can find the usage of hydraulic

* Corresponding author.

E-mail address: gilade@bgu.ac.il (E. Gilad).

<https://doi.org/10.1016/j.icheatmasstransfer.2022.106366>

Table 1
Empirical expression for C and m parameters from the literature.

Ref.	Geom. ^a	C	m	L_{ch} ^b
Hewitt and Wallis [2]	T.	0.88–1 smooth edges 0.725 sharp edges	1	D
Clift et al. [4] ^c	T.	0.79	0.34 for $L/D < 120$ $m = 0.1928 + 0.01089$ $(L/D) - 3.754 \cdot 10^{-5}(L/D)^2$ for $L/D > 120$ $m = 1$	D
Jayanti and Hewitt [9]	T.	1		D
Wu et al. [15]	A.	0.78 for $L_{ch} = D_h$ 0.56 for $L_{ch} = W$	1.7	D_h $W = (D_i + D_o)/2$ $W = \text{Width for R.}$ $W = \pi(D_i + D_o)/8$ for A.
Osakabe and Futamata [7]	A.	0.58	$m = 0.3Bo^{1/8}$, $Bo = W^2(\rho_l - \rho_g)g/\sigma$	
Drosos et al. [13]	R.	1.136	0.708	s
Sudo et al. [8]	R.	$C = 0.66(s/W)^{-0.25}$	$m = 0.5 + 0.0015Bo^{*1.3}$, $Bo^* = Ws(\rho_l - \rho_g)g/\sigma$	s
Osakabe and Kawasaki [5]	R., A.	0.58 for R. 0.38 for A.	0.8	$W = \text{Width for R.}$ $W = \pi(D_i + D_o)/2$ for A.

^a T. for Tube, A. for Annuli, R. for Rectangular.

^b Characteristic length for Eq. (1).

^c Was checked with different liquids.

diameter [15], average circumference [5], and 1/4 of average circumference [7]. Some studies explained the different definitions of the characteristic length by the different flow patterns observed in the experiments. According to Osakabe and Futamata [7], for rectangular channels, the liquid is mainly flowing at the two corner parts when the most channel width is empty for gas flow. No uniform film around the annuli circumference was detected for the annuli channel. Instead, the so-called “unit cells” around the circumference were observed as in rectangular geometry [7]. Based on the visual observation, Osakabe and Futamata [7] defined the characteristic length of annulus channels as 1/4 of the average circumference (due to four “unit cells”). However, it is not clear why for any annuli dimensions and gas and liquid velocities, there are precisely four “unit cells”.

The primary motivation for the current work is to examine which geometric dimension is the most suitable to predict the onset of flooding velocity. The main objective of the study is to derive new generalized relationships for the Wallis-type equation's parameters based on a wide range of channel geometries and dimensions. The novel generalized empirical correlation could be defined regardless of the channel geometry.

2. Empirical correlations for onset flooding velocity

Wallis [1] pioneered the use of liquid and gas dimensionless velocities to predict the onset flooding conditions according to the equation:

$$j_g^{*0.5} + m j_l^{*0.5} = C; \quad j_k^* = j_k \left[\frac{\rho_k}{gD(\rho_l - \rho_g)} \right]^{0.5}; \quad k = l \text{ or } g. \quad (1)$$

An alternative expression to the Wallis-type equation, where the gas and liquid velocities are correlated by the Kutateladze number [6], is

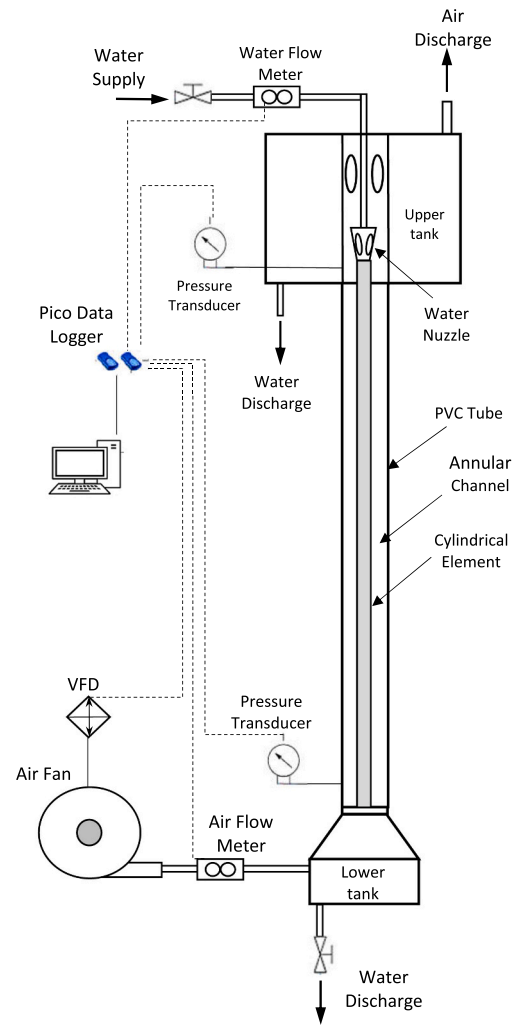


Fig. 1. Schematic view of the experimental apparatus.

defined as follows:

$$K_g^{0.5} + m_2 K_l^{0.5} = C_2; \quad K_k = j_k \left[\frac{\rho_k}{g\sigma(\rho_l - \rho_g)} \right]^{0.25}; \quad k = l \text{ or } g. \quad (2)$$

Both equations are defined using the superficial gas/liquid velocities instead of the actual velocities. Kutateladze number, K , is independent of the tube diameter and is more suitable for large diameter tubes [5]. Eq. (2) can be developed from Eq. (1) if the critical wavelength, $\lambda = [\sigma/g(\rho_l - \rho_g)]^{0.5}$, is substituted instead of the tube diameter, D , in Eq. (1). Since most of the experimental works were empirically analyzed with the Wallis-type equation, the present study will be focused only on that type expression.

Many modifications of the C and m parameters have been proposed based on specific data and ranges. Table 1 summarizes some empirical expressions of those parameters found in the literature and will be reviewed in this work. Table 1 shows a wide variation of the characteristic length used for the Wallis-type equation for rectangular and annular channel geometries. According to Jayanti and Hewitt [9], the m parameter is a parabolic function of L/D ratio. Osakabe and Futamata [7] proposed a power-law function between the m parameter and Bond number. However, it should be emphasized that in this case, the characteristic length for annular geometry was defined as 1/4 of the average circumference. Sudo et al. [8] proposed a power-law function between the m parameter and a modified Bond number ($Bo^* = Ws(\rho_l - \rho_g)g/\sigma$)

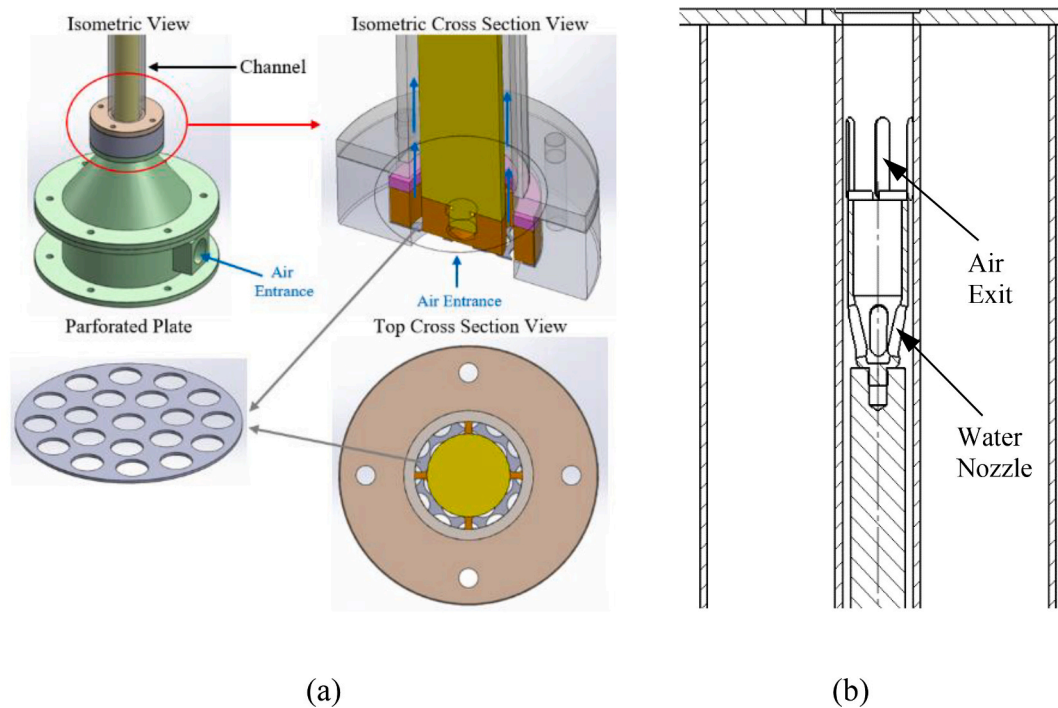


Fig. 2. The entrance and exit channel details: (a) air entrance (lower part); (b) air exit and water entrance (upper part).

and used a channel gap, s , as a characteristic length. According to Sudo et al. [8] the C parameter for a rectangular channel can be correlated by a power-law function of the channel gap to width ratio. Most studies proposed a constant value for C parameter [2,4,5,7,9,13,15], though the range is quite large (0.38–1.136). Some scattering can be explained by the effect of the pipe end geometry [10]. However, the primary reason for that wide range is the influence of the channel geometry and the variation in the characteristic length defined by different studies. For example, for the same experimental results, the C parameter varies by about 40% depending on the characteristic length definition (see, e.g., values of the C parameter in Table 1 proposed by Wu et al. [15]). It should be emphasized that all these studies analyzed a relatively small amount of geometric channel parameters. Therefore, the proposed correlations could be valid only for a narrow range of the channel geometries.

3. Experimental apparatus and procedure

A schematic view of the experimental apparatus used in this study is shown in Fig. 1. The outer tube is transparent PVC (Polyvinyl Chloride) to observe two-phase flow regimes and onset flooding conditions. The test channel is modular, so changing the channel geometric from tube to annular is possible by a different cylindrical test element inserted into the channel centrally. The air flow, controlled with Variable Frequency Drive (VFD), blows upward into the test section by a fan. The injected air passed through a digital flow meter, conical tank, and perforated plate. The water is injected through a nozzle from the top of the channel and is controlled by a needle valve. Fig. 2 describes the test channel entrance and exit details. A perforated plate with a ratio of the total holes area to the channel cross-section area of 65% was located at the channel entrance to stabilize the air velocity distribution. The air is discharged from the channel through a hatch above the water-injected nozzle. The water can be discharged through the upper or lower collector tanks (see Fig. 1). Two pressure transducers were installed, one at the bottom and the other at the top of the channel (below the water nozzle), to measure the pressure gradient concerning the environment. All the measurement instrumentation was calibrated. The air and water flow meters are newly

Table 2
Main experimental components and instrumentation details.

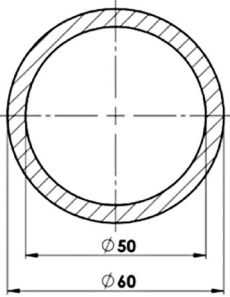
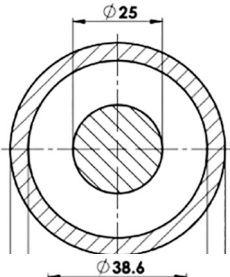
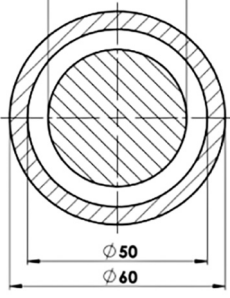
Component	Model &Details
Air Fan	Model: Regenerative two-stage B-820, direct drive Properties 11 kW, 3500 rpm, 60 Hz Pressure range: 0–750 mbar Air Flow rate: 0–650 m ³ /h
Air flow meter	CS Instruments GmbH & Co. KG, Model: VA 500 Flow rate range: 0–600 m ³ /h Flow rate velocity: 0–90 m/s Accuracy: $\pm 1.5\%$ m.v., $\pm 0.3\%$ f.s Smar, Model: LD301
Pressure transducer	Range: 0–250 mbar, 0–50 mbar Accuracy: $\pm 0.04\%$
Water flow meter	EGE, Model: SDN 552/1 GAPP Range: 0–10 lit/min Accuracy: $\pm 1.5\%$
PicoLog Data Logger	Pico Technology, Model: PicoLog 1000 Resolution: 16 bits Sampling rates: 1 MS/s Accuracy: $\pm 0.5\%$
VFD (Variable Frequency Drive)	ABB, Model: ACS – 580 Range: 75–500 HP Max. Frequency: 500 Hz

purchased and arrived after a manufacturer calibration. The gas/liquid flow rate data and the pressure gradient on the test element were collected and saved using a PC by a data logger model Picolog 1000 of PICO Technology Company.

The current system is different and unique compared to other experimental works. While most previously published experimental works used the gravitational water feeding method, in this study, the liquid injection is forced at a constant flow rate through a nozzle, which distributes the liquid peripherals into the flow channel. This configuration best simulates the operation of an Emergency Core Cooling System (ECCS), as found in some nuclear fuel rod designs.

Table 2 summarizes the main experimental components and instrumentation details. All the experiments were conducted at the same pressure and temperature conditions. The system pressure was around

Table 3
Channels details and experimental conditions.

Num.	Description	Channel cross section geometry	j_b , m/s	j_g , m/s	D_h , mm	W , mm	L , mm
1	Tube		0–0.1	0–15	50	78.5	1500
2	Annular		0–0.1	0–15	25	117.8	1500
3	Annular		0–0.2	0–15	11.4	139.2	1500

the atmospheric, and the inlet water and air temperatures along the entire channel length were 20–30 °C.

The current work tested one tube and two annular (with different inside diameters) channel cross-sections. All three channels have 1500 mm length (from the perforated plate up to the water nozzle) and the same external pipe. The tube channel has 50 mm I-D, and the annular channels have hydraulic diameters of 25 mm and 11.4 mm and an average circumference of 117.8 mm and 139.2 mm, respectively. The cross-section channel geometric details and the experimental conditions are summarized in Table 3. The tested channel geometries were chosen so that the hydraulic diameter trend is inverse to the average circumference; therefore, the most representative characteristic length could be found by comparing the results of different channels.

The experimental procedure includes several stages. In the first stage, a constant water flow rate (for several predetermined values) was injected downward from the top of the channel. For the second stage, a low air flow rate was blown into the test channel, and the counter-current flow regime was achieved, simulating an emergency cooling systems activation. When the system was stabilized, the air flow rate was

gradually increased by changing the engine frequency of the fan engine. The system's steady-state conditions were ensured, and all the data was collected before any air flow rate change. The point where the first droplets of water drift up and discharge from the exit hatch (Fig. 2(b)) is defined as the onset of flooding. Most researchers accept this definition. The onset flooding condition might also be found by following the pressure gradient above the water entrance when the pressure gradient surges significantly for the onset flooding. All measured data were collected and saved every second for further analyses using a PC by a Pico data logger.

Since the external pipe of the test channel was made of transparent PVC, it was possible to visualize the two-phase flow regime for different experiments. According to our observation, the two-phase flow regime transformation due to increasing air velocity is almost the same for tube and annular channels. As the air flow rate increased, the two-phase flow changed from steady counter-current annular to chaotic (churn flow) on the channel bottom with the annular flow on the middle and upper parts. Further increase in the air flow rate resulted in the expansion of the churn flow region and a slug flow (which represents the onset flooding

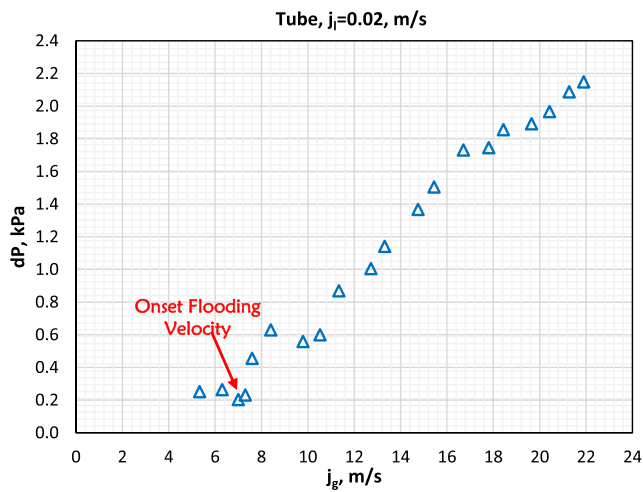


Fig. 3. Typical measurement results of the differential pressure versus gas velocity.

and partial water delivery). For relatively high water velocity, the onset flooding occurs due to the “top flooding” when the water enters from the nozzle exit before it reaches the test channel. It should be mentioned that even for the high water velocity cases, the difference between the channel slug flow flooding and the top flooding is not significant in the air velocity term. Finally, the flow regime reaches concurrent upward flow.

Fig. 3 presents typical results of the differential pressure versus gas velocity for onset flooding velocity measured in the tube channel. The upper transducer measured the pressure gradient (see Fig. 1) concerning the environment. Fig. 4 presents the evolution of the flow regimes observed in an annular channel (see channel Num. 3 in Table 3) for the same water superficial velocity ($j_l = 0.126$ m/s) when the air velocity gradually increases. The pictures from left to right represent an annular counter-current flow regime, churn flow regime on the channel bottom with the annular flow on the middle and upper parts, slug flow regime (onset flooding), and concurrent upward flow regime, respectively.

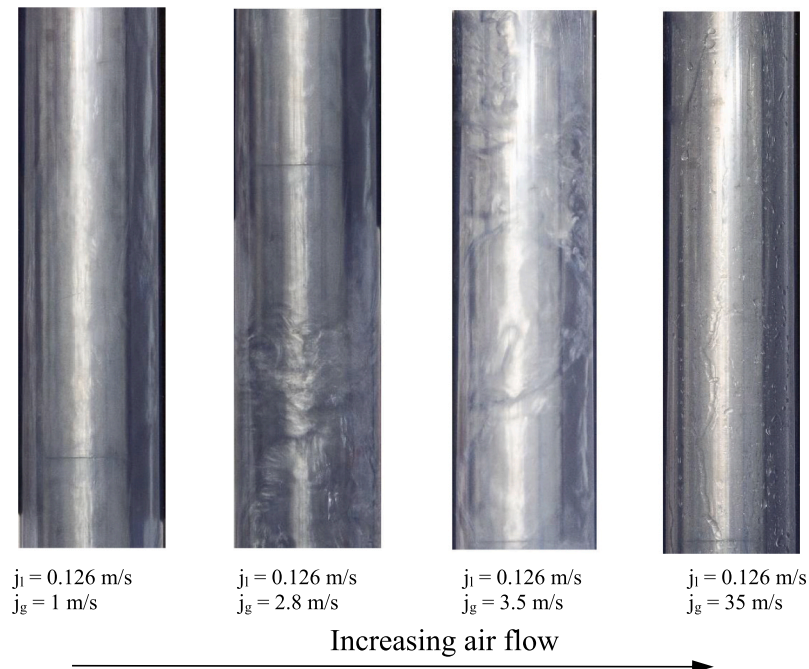


Fig. 4. Two-phase flow regimes observed during increasing air velocity in the annular channel.

4. Experimental results and discussion

Fig. 5 presents the experimental results for the onset of flooding conditions for three different channel geometries conducted in this study. All three channels have shown the same trend for which the air superficial velocity decreased by increasing the water flow rate. The decreasing air velocity trend for low water flow rates is steeper than for high values.

The uncertainty of the experimental results was calculated according to the method of Kline and McClintock [18]. The air velocity was measured at some distance from the channel entrance (see Fig. 1). Thus, the measured values were recalculated based on the actual absolute pressure measurements on the channel entrance and the ideal gas and mass conservation laws. Apart from the accuracy of the system components (see Table 2), additional manufacturing errors were considered as channel diameter ± 0.1 mm. The variations in air and water thermophysical properties, such as density, were neglected since all

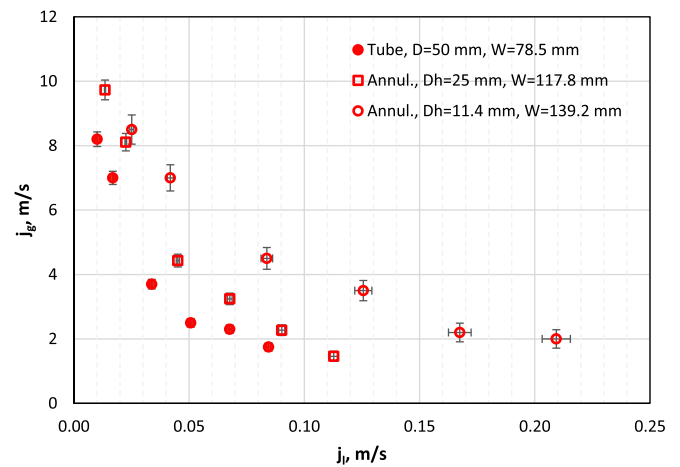


Fig. 5. Experimental results for the onset of flooding conditions conducted using three different channel geometries.

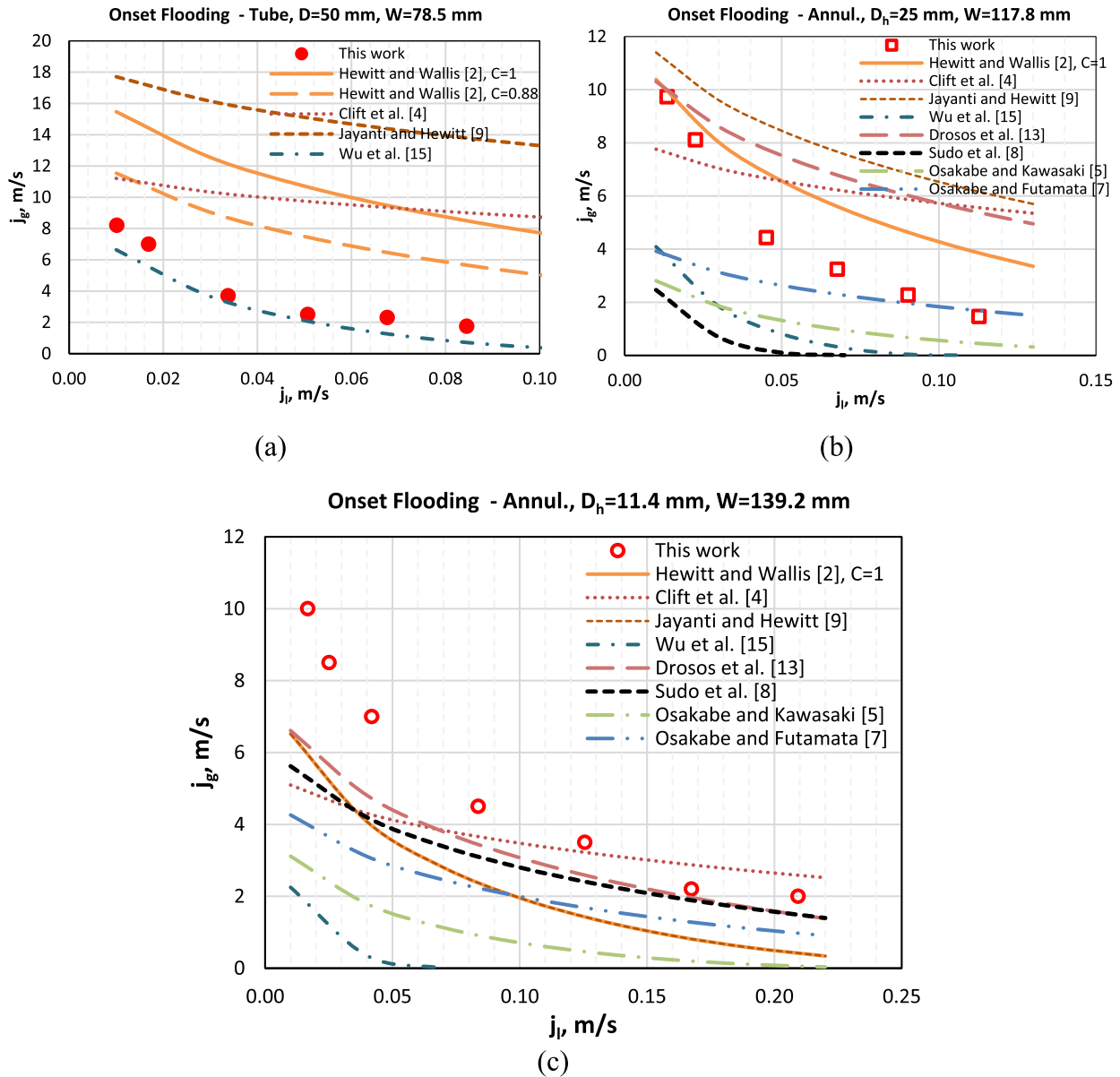


Fig. 6. Comparison between empirical correlations (see Table 1 and Eq. (1)) for the onset of flooding and experimental results: (a) Tube, $D = 50$ mm, $W = 78.5$ mm; (b) Annul., $D_h = 25$ mm, $W = 117.8$ mm; (c) Annul., $D_h = 11.4$ mm, $W = 139.2$ mm.

experiments were conducted at the same temperature. The total calculation of the system uncertainty showed a maximum of 3.5% for water velocity and 14% for low-range air velocity. The relative uncertainty of the air velocity decreased by increasing the channel hydraulic diameter and velocity, whereas, for high air velocity values, the uncertainty is only 3–5%.

Fig. 6 presents the experimental results of this study compared with the empirical correlations from the literature (see Table 1). None of the proposed correlations fit all three channel geometries. The correlation of Wu et al. [15] seems to be the closest to the tube experiments (11%–59% deviation); however, the agreement is not good for the other two geometries. The most suitable correlation for two annular geometries is Osakabe and Futamata [7], with a difference of about 0–60%. An important conclusion can be derived by comparing the flooding velocity values predicted by the correlations with experimental results. For those correlations defined by a hydraulic diameter or channel gap (as a characteristic length) [2,4,9,13], the predicted flooding velocity decreases for annular channels due to the decrease in hydraulic diameter.

On the contrary, for the correlations defined by average circumference (as a characteristic length) [5,7], the flooding velocity increases for annular channels due to the circumference increase.

The air flooding velocity from various studies was presented as a function of W and D_h as shown in Fig. 7, to make a more educated selection of the most suitable characteristic length for onset flooding conditions. All the previous results were obtained in the same range $j_l = 0.085 - 0.11$ m/s, however, with various channel shapes and dimensions. Based on Fig. 7(a), there is a clear correlation between the onset of flooding velocity and W . Increasing W results in increased j_g for both annular and rectangular channels. As presented in Fig. 7(b), no clear trend can be identified by comparing the experimental results regarding hydraulic diameter for annular and rectangular channels. Based on the comparisons from Figs. 5–7, the hydraulic diameter cannot be used as a characteristic length for annular and rectangular channels. Instead, the average circumference for the annular channel or channel width for the rectangular channel is a more appropriate parameter. Moreover, according to Fig. 6, the C and m parameters from the Wallis-

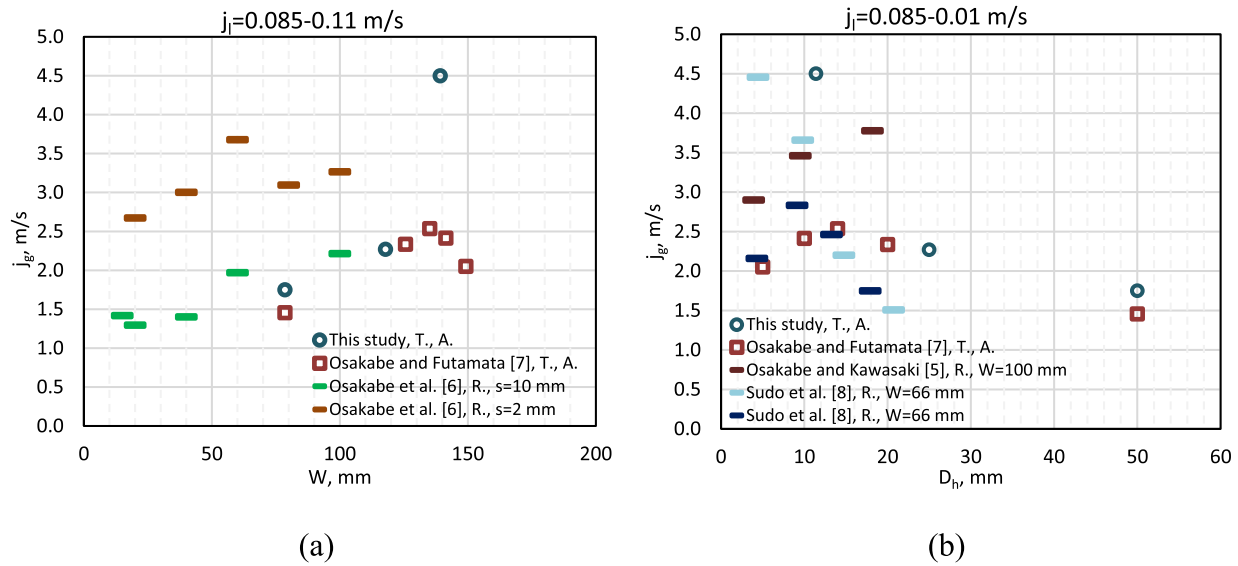


Fig. 7. Onset flooding air velocity for $j_l = 0.085 - 0.11$ m/s : (a) j_g vs. W ; (b) j_g vs. D_h .

Table 4

Experimental conditions for onset flooding from the current study and the literature.

Ref.	Geom. ^a	D_i , mm	D_o , mm	s , mm	D_h , mm	W , mm	L , mm
This study	A.	25–38.6	50	5.7–12.5	11.4–25	117.8–139.2	1500
Wu et al. [15]	A.	70	170	50	100	377	2000
Osakabe & Futamata [7]	A.	16–45	50	2.5–17	5–34	33–47.5	350
Osakabe & Kawasaki [5]	R.	–	–	2–10	4–20	100	1235
Drosos et al. [13]	R.	–	–	10	20	120	380
Vlachos et al. [12]	R.	–	–	5–10	10–20	150	400
Osakabe et al. [6]	R.	–	–	2–10	4–20	20–100	150–1200
Sudo et al. [8]	R.	–	–	2.3–12.3	4.6–24.6	33–66	362–782
This study	T.	–	–	–	50	78.5	1500
Osakabe & Futamata [7]	T.	–	–	–	50	78.5	350
Wallis et al. [3]	T.	–	–	–	25.4	39.9	292
Kusunoki et al. [14] ^b	T.	–	–	–	20	31.4	500
Zapke and Kroger [11] ^b	T.	–	–	–	30	47.1	2000
Jeong and No [10] ^c	T.	–	–	–	30	47.1	500–2000

^a T. for Tube, A. for Annuli, R. for Rectangular.

^b Was checked initially with different liquids. For that study, only air-water results were analyzed.

^c Only rounded water entrance and sharp water exit (see BJ in [10]) were considered.

type equation should be further investigated to find more suitable relationships.

5. Empirical analysis of Wallis-type equation parameters

To find a generalized expression for the Wallis-type equation m and C parameters, various experimental results for different channel shapes and dimensions were arranged and analyzed. Table 4 summarizes the experimental conditions for onset flooding from the current study and the literature. Three studies were conducted with annular channels, including channel gap, s , in the range of 2.5–50 mm, average circumference, $W = \pi(D_o + D_i)/2$, in the range of 33–377 mm and channel length, L , in the range of 350–2000 mm. Five studies were conducted with rectangular channels, including channel gap, s , in the range 2–12.3 mm, channel width, W , in the range 20–150 mm, and channel length, L , in the range 150–1235 mm. Six studies were conducted with circular tubes, including tube diameter, D_h , in the range of 20–50 mm and channel length, L , in the range 292–2000 mm. It should be mentioned that Jeong and No [10] originally presented different results for various pipe end geometries. For comparison purposes with the rest of the studies presented in Table 4, most of which employ rounded water entrance and sharp water exit, only experiments with similar pipe end

geometries were considered from Jeong and No [10].

Only a few studies analyzed (parametrically) the influence of geometrical dimensions on the Wallis-type equation C and m parameters. Osakabe and Kawasaki [5] studied the influence of the channel gap and the average circumference for annular channel geometry, Osakabe et al. [6] and Sudo et al. [8] studied the influence of rectangular channel gap, width and length, and Jeong and No [10] studied the influence of circular tube length. Based on the results of Osakabe et al. [6], Sudo et al. [8], and Jeong and No [10], there is almost no influence (or the influence is not consistent) of the channel length on both parameters, C and m . According to Sudo et al. [8] and Osakabe et al. [6], the m parameter increased by increasing the W . Sudo et al. [8] also found that the m parameter increased by increasing the channel gap, s . The influence of geometrical dimensions on the C parameter is inconsistent throughout the studies. One of the possible reasons for that is the variation of the characteristic length used in different studies for the Wallis-type equation. To compare different studies, the results for rectangular and annular channels defined by the hydraulic diameter or channel gap such as [8,13] were recalculated based on the channel width or average circumference, W , respectively. By replacing the characteristic length from the hydraulic diameter or channel gap to W , the m parameter does not change. However, the C parameter is decreased by the ratio $(D_h/$

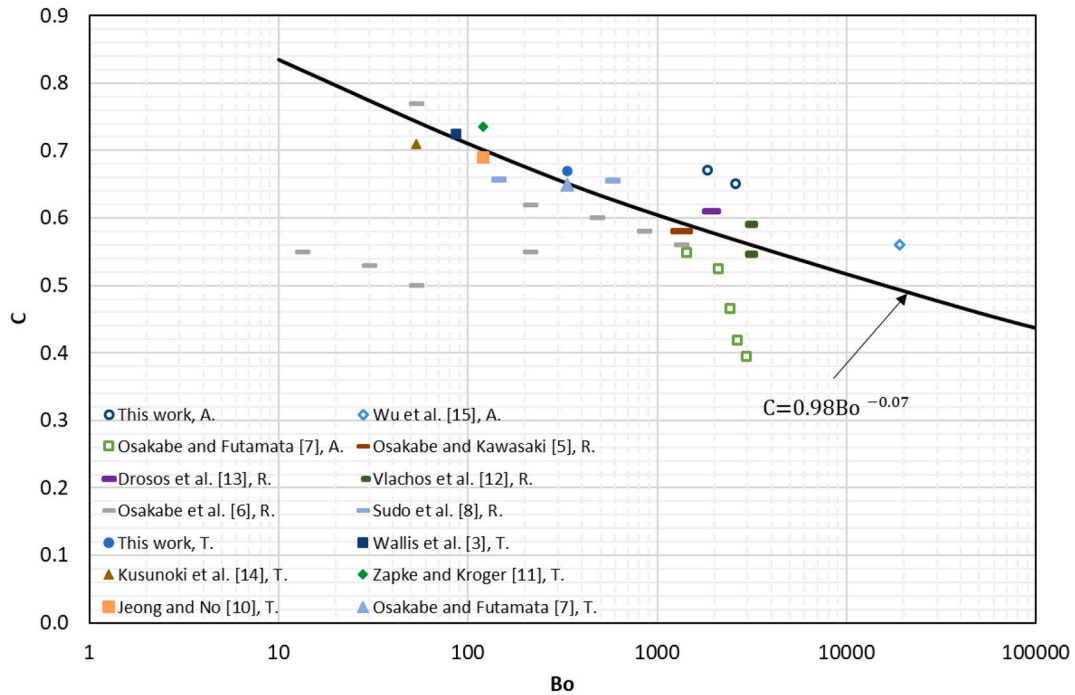


Fig. 8. Relation between the C parameter and the Bond number.

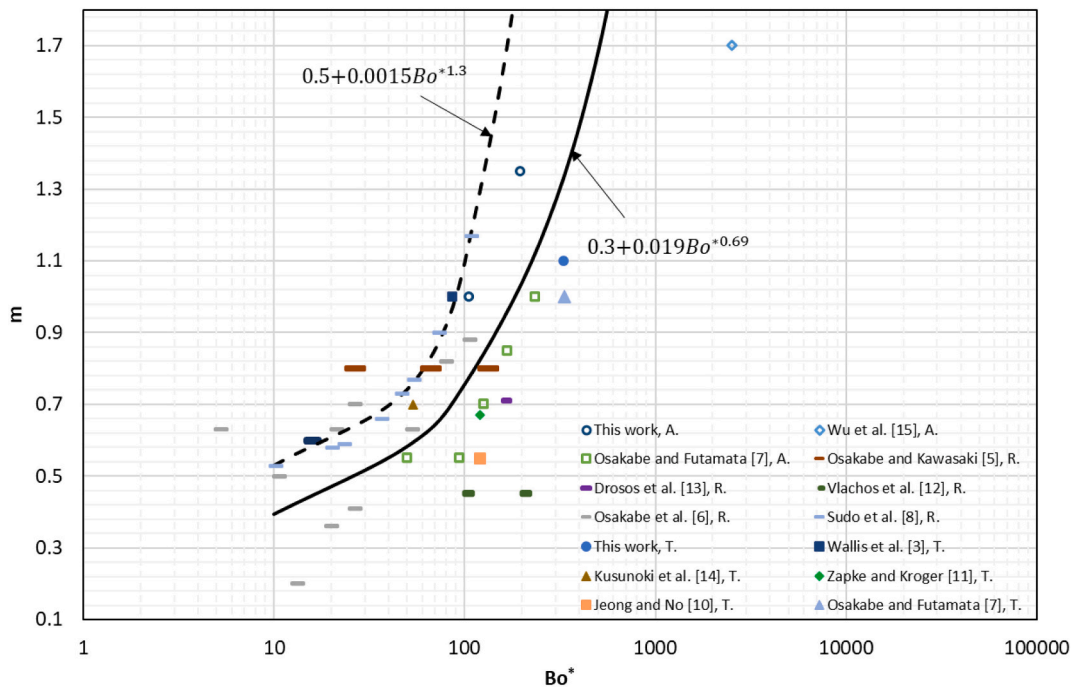


Fig. 9. Relation between the parameter m and the modified Bond number.

$W^{0.25}$ or $(s/W)^{0.25}$, respectively. For example, the original value of 1.52 for C parameter found in a rectangular channel with a gap of 2.3 mm and width of 66 mm [8] becomes approximately 0.66.

As shown in Table 1, some studies [7,8] choose to present the m parameter in the Wallis-type equation as a function of the Bond number, Bo . The Bond number describes the ratio of gravitational and surface forces, the dominant forces in the flooding phenomena. Therefore, it may not be unreasonable to describe the C and m parameters in terms of the Bond number. The Bond number can also be represented as the square ratio of characteristic length and the critical wavelength, λ , as

follows [7]:

$$Bo = \frac{L_{ch}^2 (\rho_l - \rho_g) g}{\sigma} = \left[\frac{L_{ch}}{\lambda} \right]^2; \quad (3)$$

$$\lambda = \left[\frac{\sigma}{g(\rho_l - \rho_g)} \right]^{0.5}$$

Based on the empirical analysis of experimental results from Table 4, the C parameter could be presented as a function of the Bond number, see Fig. 8, according to the relation:

$$C = 0.98Bo^{-0.07} \quad (4)$$

Where the characteristic length, L_{ch} , for the Bond number is defined as:

$$L_{ch} = W \text{ for A. and R.}; L_{ch} = D \text{ for T.}$$

$$W = \pi(D_i + D_o)/2 \text{ for A.}; W = \text{Width for R.} \quad (5)$$

The m parameter was best fitted with the modified Bond number, as shown in Fig. 9. The points related to the annular, rectangular, and tube channels seem to be well predicted by the relation (thick line):

$$m = 0.3 + 0.019Bo^{*0.69} \quad (6)$$

Where the modified Bond number, Bo^* , is defined as [8]:

$$Bo^* = \frac{Ws(\rho_l - \rho_g)g}{\sigma} \text{ for R. and A.};$$

$$Bo^* = Bo = \frac{D^2(\rho_l - \rho_g)g}{\sigma} \text{ for T.} \quad (7)$$

Fig. 9 also presents the m parameter relation proposed by Sudo et al. [8] (see Table 1) for comparison (dashed line). Some scattering could be explained from various experimental facility details, like water and air inlet paths. The results for large annular channels seem out of the primary trend and should be further investigated.

6. Conclusion

This work presents new experimental results and analyses for the onset of flooding conditions. The test facility included a transparent PVC vertical tube of 50 mm inside diameter and modular inserts to investigate various annular channel geometries. By comparing multiple empirical correlations from the literature with the experimental results from this study and previously published works, it was found that for annular and rectangular channels, the hydraulic diameter (D_h) could not be used as a characteristic length. Instead, an average circumference and channel width (W) may be used. None of the found correlations predicted well all channel geometries. We propose new general empirical relations for C and m parameters of the Wallis-type equation by analyzing twelve different experimental studies, including annular, rectangular, and circular channels with a wide range of geometric dimensions. We found that the C parameter has a power-law relation with the Bond number and that the modified Bond number may be used to evaluate the m parameter.

Nomenclature

A., R., T.	A. for Annulus, R. for Rectangular, T. for Tube
C, m	Wallis-type equation parameters (Eq. (1))
Bo	Bond number, $= L_{ch}^2(\rho_l - \rho_g)g/\sigma$
Bo^*	Modified Bond number, $= Ws(\rho_l - \rho_g)g/\sigma$
C_2, m_2	Kutateladze type equation parameters (Eq. (2))
D	Tube diameter, m
D_h	Hydraulic diameter, m
g	Gravitational acceleration, m/s ²
j	Superficial velocity, m/s
j^*	Nondimensional superficial velocity, $j_k^* = j_k[\rho_k/gL_{ch}(\rho_l - \rho_g)]^{0.5}$
K	Kutateladze number (Eq. (2))
L	Channel length, m
L_{ch}	Characteristic length, m
P	Pressure, bar
s	Channel gap, m
W	Average circumference for an annuli channel or channel width (wider span) for a rectangular channel, m

Greek symbols

ρ	Density, kg/m ³
σ	Surface tension, N/m
λ	Critical wavelength, m, $[\sigma/g(\rho_l - \rho_g)]^{0.5}$

Subscript

l	liquid
g	gas
i	inside
o	outside

Acronyms

PVC	Polyvinyl Chloride
LOCA	Loss of Cooling Accident
ECCS	Emergency Core Cooling Systems
VFD	Variable Frequency Drive

CRediT authorship contribution statement

A. Biton: Conceptualization, Methodology, Formal analysis, Investigation, Resources, Data curation, Writing – original draft. **E. Rabino-**
vich: Conceptualization, Methodology, Formal analysis, Investigation, Resources, Writing – original draft, Supervision. **E. Gilad:** Conceptualization, Methodology, Supervision, Writing – review & editing, Project administration.

Declaration of Competing Interest

The authors declare that they have no known competing financial interests or personal relationships that could have appeared to influence the work reported in this paper.

Data availability

Data will be made available on request.

References

- [1] G.B. Wallis, One Dimensional Two-Phase Flow, McGraw-Hill, New York, 1969.
- [2] G.B. Wallis, Flooding and Associated Phenomena in Falling Flow in a Vertical Tube, UKAEA Report No. AERE-R4022, HMSO, London, 1963.
- [3] G.B. Wallis, A.S. Karlin, C.R. Clark, D. Bharathan, Y. Hagi, H.J. Richter, Countercurrent gas-liquid flow in parallel vertical tubes, Int. J. Multiphase Flow 7 (1981) 1–19.
- [4] R. Clift, C.L. Pritchard, R.M. Nedderman, The effect of viscosity on the flooding conditions in wetted wall columns, Chem. Eng. Sci. 21 (1966) 87–95.
- [5] M. Osakabe, Y. Kawasaki, Top flooding in thin rectangular and annular passages, Int. J. Multiphase Flow 15 (5) (1989) 747–754.
- [6] M. Osakabe, T. Kubo, H. Baba, Top flooding in thin rectangular channels, JSME Int. J. 37 (3) (1994) 491–496.
- [7] M. Osakabe, H. Futamata, Effect of inserted rod and cross flow on top flooding of pipe, Int. J. Multiphase Flow 22 (5) (1996) 883–891.
- [8] Y. Sudo, T. Usui, M. Kaminaga, Experimental study of falling water limitation under a counter-current flow in a vertical channel (first report, effect of flow channel configuration and introduction of CCFL correlation), JSME Int. J. Series II (34) (1991) 169–174.
- [9] S. Jayanti, G.F. Hewitt, Prediction of the slug to churn flow transition in vertical two phase flow, Int. J. Multiphase Flow 18 (6) (1992) 847–860.
- [10] J.H. Jeong, H.C. No, Experimental study of the effect of pipe length and pipe-end geometry on flooding, Int. J. Multiphase Flow 22 (3) (1996) 499–514.
- [11] A. Zapke, D.G. Kroger, The influence of fluid properties and inlet geometry on flooding in vertical and inclined tubes, Int. J. Multiphase Flow 22 (3) (1996) 461–472.
- [12] N.A. Vlachos, S.V. Paras, A.A. Mouza, A.J. Karabelas, Visual observation of flooding in narrow rectangular channels, Int. J. Multiphase Flow 27 (2001) 1415–1430.
- [13] E.I.P. Drosos, S.V. Paras, A.J. Karabelas, Counter-current gas-liquid flow in a vertical narrow channel-liquid film characteristics and flooding phenomena, Int. J. Multiphase Flow 32 (2006) 51–81.

- [14] T. Kusunoki, M. Murase, Y. Fujii, T. Nozue, K. Hayashi, S. Hosokawa, A. Tomiyama, Effects of fluid properties on CCFL characteristics at a vertical pipe lower end, *J. Nucl. Sci. Technol.* 52 (6) (2015) 887–896.
- [15] B. Wu, M. Firouzi, T.E. Rufford, B. Towler, Characteristics of counter-current gas-liquid two-phase flow and its limitations in vertical annuli, *Exp. Thermal Fluid Sci.* 109 (2019) 1–17.
- [16] Kh. Hosseinzadeh, D.D. Ganji, F. Ommi, Effect of SiO₂ super-hydrophobic coating and self-rewetting fluid on two-phase closed thermosyphon heat transfer characteristics: an experimental and numerical study, *J. Mol. Liq.* 315 (2020), 113748.
- [17] Kh. Hosseinzadeh, M.A.E. Moghaddam, M. Hatami, D.D. Ganji, F. Ommi, Experimental and numerical study for the effect of aqueous solution on heat transfer characteristics of two-phase closed thermosyphon, *Int. Commun. Heat Mass Transf.* 135 (2022), 106129.
- [18] S.J. Kline, F.A. McClintock, Describing uncertainties in single sample experiments, *Mech. Eng.* 75 (1953) 3–8.